New Tracers and Detection Methods

Article available at http://www.epj-conferences.org or http://dx.doi.org/10.1051/epjconf/20135005001

EPJ Web of Conferences **50**, 05001 (2013)
DOI: 10.1051/epjconf/20135005001

PEPT: An invaluable tool for 3-D particle tracking and CFD simulation verification in hydrocyclone studies

Yu-Fen Chang[1,a], Tom C.H. Adamsen[2,3,b], Gleb I. Pisarev[1,c] and Alex C. Hoffmann[1,d]

[1] *University of Bergen, Department of Physics and Technology, Allegaten 55, 5007 Bergen, Norway*
[2] *Centre for Nuclear Medicine and PET, Department of Radiology, Haukeland University Hospital, Jonas Liesvei 65, 5021 Bergen, Norway*
[3] *University of Bergen, Department of Chemistry, Allegaten 41, 5007 Bergen, Norway*

Abstract. Particle tracks in a hydrocyclone generated both experimentally by positron emission particle tracking (PEPT) and numerically with Eulerian-Lagranian CFD have been studied and compared. A hydrocyclone with a cylinder-on-cone design was used in this study, the geometries used in the CFD simulations and in the experiments being identical. It is shown that it is possible to track a fast-moving particle in a hydrocyclone using PEPT with high temporal and spatial resolutions. The numerical 3-D particle trajectories were generated using the Large Eddy Simulation (LES) turbulence model for the fluid and Lagrangian particle tracking for the particles. The behaviors of the particles were analyzed in detail and were found to be consistent between experiments and CFD simulations. The tracks of the particles are discussed and related to the fluid flow field visualized in the CFD simulations using the cross-sectional static pressure distribution.

1. INTRODUCTION

1.1. Positron emission particle tracking (PEPT)

Positron emission particle tracking (PEPT), a technique to follow moving particles 3-dimensionally, has been applied to studies of flow systems and processes, e.g. fluidized bed (see, e.g., Ref. [1]), pharmaceutical coating process [2], casting process [3], and processing of solid-liquid food mixtures [4]. In addition to laboratory experiments, on-site particle tracking in a pressurized fluidized bed at BP's Hull Research and Technology Center using a portable PEPT camera was demonstrated by Ingram et al. [5]. Different phases can be tracked and studied, e.g. the flows of fluids can be visualized by following neutral density particles, i.e. particles having a similar density to the fluids. Due to the principle used, PEPT serves well in opaque and turbid systems.

PEPT employs the same principle as the medical imaging technique Positron Emission Tomography (PET). The differences lie in the nature of the tracked objects, the data processing and, as a consequence, the resolutions achievable. In PET the spatial distribution of a cloud of tracer is studied using image reconstruction techniques, while in PEPT a point-like tracer is located. PET needs enough counts for processing statistically meaningful histograms and images, whereas theoretically PEPT needs only few events for positioning the tracer. Therefore PEPT can achieve higher temporal and spatial resolution, for example Wildman et al. [6] achieved a temporal resolution of 2 ms with a spatial accuracy of about 1 mm. In this paper, we report particle tracking using a Siemens TruePoint PET camera and an in-house developed data-processing algorithm. A temporal resolution down to 1 ms is easily obtainable with a spatial resolution of 0.33 mm. Particle trajectories in a hydrocyclone are presented and compared with those obtained by CFD (computational fluid dynamics) simulation.

[a] e-mail: yu-fen.chang@ift.uib.no
[b] e-mail: tom.christian.holm.adamsen@helse-bergen.no
[c] e-mail: gleb.pisarev@ift.uib.no
[d] e-mail: alex.hoffmann@ift.uib.no

1.2. Hydrocyclone separator

With the main merits of simple construction, fairly high efficiency, and continuous operation capability, cyclones are extensively used for separation or classification of phases according to density, e.g. for gas-solid, liquid-solid, and liquid-liquid separations, where the cut-size requirement for the dispersed phase particles (bubbles, drops or solid particles) is down to a few μm [7,8]. Whenever the carrier phase is a liquid, they are referred to as hydrocyclones. Cyclones have two main types of geometries: swirl tubes and cylinder-on-cone designs. Varying in shape arrangement and operating conditions, hydrocyclones can be designed for liquid-liquid separation, e.g. de-oiling hydrocyclones, and liquid-solid separation, e.g. desanding hydrocyclone, the latter of which is the focus of this study.

In conventional cylinder-on-cone, tangential-inlet cyclones, the mixture enters the cyclone tangentially, forming the outer vortex, as shown in Figure 1. The mixture then swirls toward the bottom of the conical section. The denser phase, e.g. solid particles, experiencing a "centrifugal force", moves toward the wall and leaves the cyclone through the particle outlet (also called underflow outlet). The lighter phase moves toward the central axis, forming an "inner vortex", and leaves the cyclone through the vortex finder. The pressure drop and the separation efficiency for a given dynamically equivalent particle size, namely the collected mass over feed mass, are the most important concerns in the design and application of cyclones. The performance of cyclones is influenced by details of the flow behavior and the interaction between

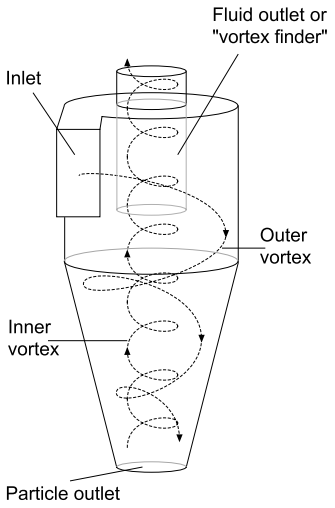

Figure 1. Cyclone separator with cylinder-on-cone design.

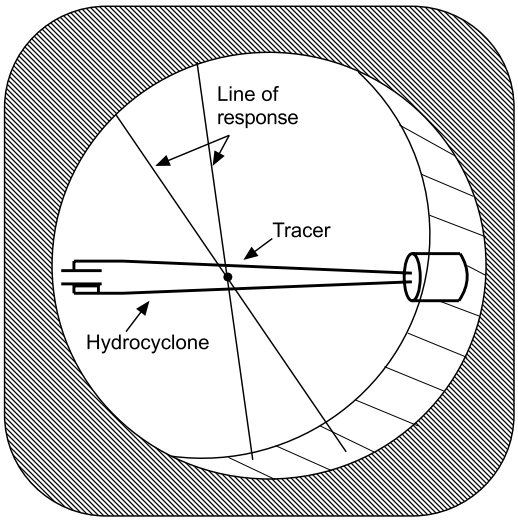

Figure 2. A schematic showing the hydrocyclone surrounded by gamma-ray sensors, the tracer, and the LORs.

different phases, which can be investigated by visualizing the trajectories of particles and fluid elements, the latter represented by neutral density particles. The trajectories of particles are helpful for understanding the separation process and potential problems, e.g. long residence time and clogging, as well as for instigating and verifying new and improved cyclone designs.

Experimentally, particle tracks in hydrocyclones have been acquired using optical setups. Knowles et al. [9] recorded 3-D positions of an anisole droplet acting as a neutral density tracer particle in a hydrocyclone using multi-directional cine-photography. Wang et al. [10] tracked a seed used as a tracer for the solid phase in a hydrocyclone two-dimensionally by means of a high-speed camera. These techniques have provided valuable flow patterns as functions of cyclone geometries and operation conditions, and elucidated efficiencies. However, how the flow behavior and consequently the separation efficiency are influenced by some special phenomena, e.g. the "end of the vortex" [11], often appearing in the complex, highly turbulent flows in cyclones, or some other cyclone-specific flow disturbance or feature is very difficult to observe. For this type of detailed information, techniques with higher temporal and spatial resolutions are required.

1.3. Particle tracking in hydrocyclones using CFD

CFD is increasingly applied for improving the design and separation efficiency of cyclones. Numerically, particles or fluid elements in hydrocyclones can be followed through space and time in a Lagrangian frame of reference. How the particle routes are affected by various parameters, e.g. particle size, entry point, and feed concentration, has been numerically studied using a variety of turbulence models (see, e.g., Ref. [12–15]). For example, Hsieh and Rajamani [12] simulated 2-D trajectories of limestone particles in a water hydrocyclone using Lagrangain particle tracking in a pre-calculated flow field. The CFD simulations of Cullivan et al. [14], based on a second-order-accurate pressure-strain Reynolds-stress turbulence model, showed particles being subjected to recirculatory paths in a hydrocyclone. Comparing trajectories obtained from various CFD models with experimental observations is important for examining the validity of the CFD models and understanding the experimental findings. In the present investigation, CFD models of a hydrocyclone were build to be consistent with the geometry used in PEPT experiments and the trajectories obtained in both are compared in detail.

2. EXPERIMENTAL

2.1. Positron emission particle tracking (PEPT)

The labelling and detection principle in PEPT are, as mentioned above, the same as that used in medical PET [16]. The tracers, which in PEPT are point-like, are labelled with isotopes containing surplus protons and undergoing positive beta decay, where a positron is emitted. After traveling a certain distance (less than 2.4 mm in water [16]), the positron annihilates with an electron, which causes the emission of two gamma photons of 511 keV each, heading in nearly 180-degree opposite directions. As these back-to-back emitted gamma photons are detected by two sensors, the tracer is known to be located somewhere along the line drawn between the sensors, referred to as the line of response (LOR). By cross-triangulation, the location of tracer can be estimated to be the cross-points, i.e. cutpoints (or points of closest proximity due to the scatter inherent in the process), of two or more LORs. Figure 2 schematically shows the gamma photons emanating from a tracer in a hydrocyclone and LORs are drawn between the locations of the detecting sensors.

To create a tracer particle strong base anion exchange resin beads "Amberlyst A26 Hydroxide Form" (Acros Organics) with sizes from 390 to 810 µm as shown in Figure 3 were immersed into the ^{18}F-contained water for about 10 minutes. ^{18}F ions are taken up through ion-exchange when the solution fills and covers the macroreticular, porous beads. In order to maximize the radioactivity on the tracer, the immersion time should

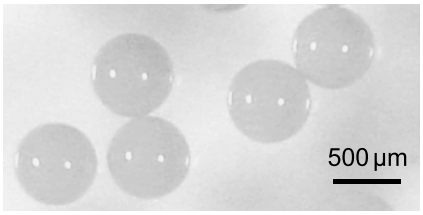

Figure 3. The strong base anion exchange resin beads used in these experiments.

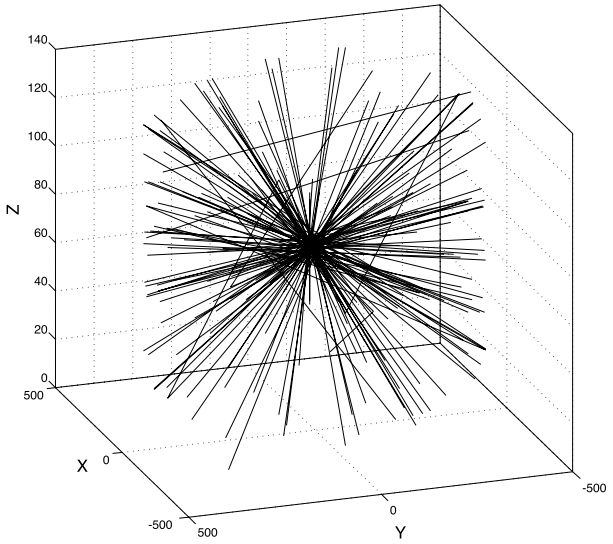

Figure 4. A 3-dimensional view of LORs emanating from a stationary resin bead during about 0.14 millisecond (z-direction expanded).

not exceed 25 minutes and the time between labelling and tracking experiments should be limited, considering the half life of ^{18}F of 109.8 minutes. By this procedure the radioactivity on a single resin bead could reach 450–1440 µCi depending on the concentration of ^{18}F in the solution and the size of the bead.

The gamma-ray sensor array used is a Siemens TruePoint PET scanner with an energy window of 425–650 keV and a coincidence window of 4.5 nanoseconds. The scanner consists of 39 rings of diameter 855.2 mm. Each ring contains 624 lutetium oxyorthosilicate (LSO) scintillation crystal sensors with dimensions of 4 mm × 4 mm × 20 mm. The coincidence window is a narrow time window intending to bracket two signals emitted from one annihilation event. Two photons detected within a coincidence window constitute one LOR. The data from the scanner, stored in "list-mode format", consist of event words, where the information of sensor location is stored. Between the event words, the scanner inserts periodic timing words every millisecond into the data stream. The position of the tracer every millisecond can be determined by finding the best average of the cutpoints of the numerous LORs. Figure 4 shows LORs from a stationary tracer during about 0.14 millisecond, with the z-direction being expanded. Some false LORs appear mainly because the scanner once in a while detects only one of the pair photons from each of two events that both take place within the same coincidence window. An algorithm developed by Hoffmann et al. [17] to eliminate the false cutpoints was

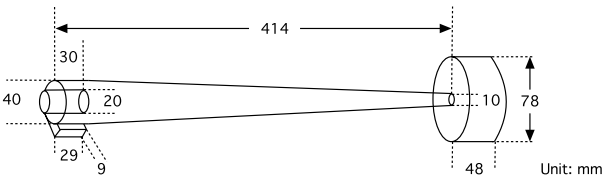

Figure 5. The dimensions of hydrocyclone used in this study.

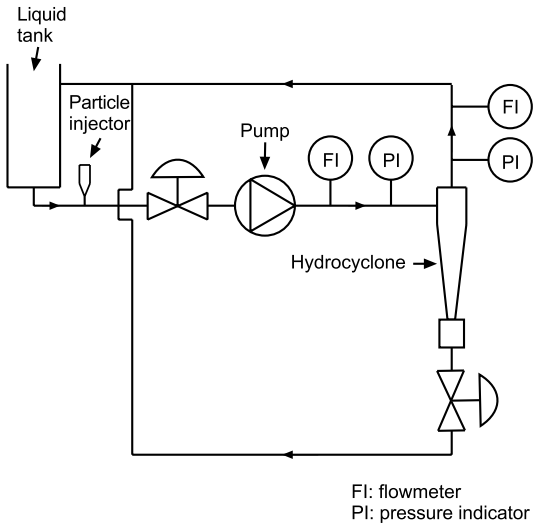

Figure 6. The hydrocyclone in a recirculation system.

tailored and implemented in a Fortran program for this present project.

The concept of the positioning algorithm is as follows [17]. The LOR cutpoints in the x-y-plane are considered first. The first estimation of the particle position in this plane is obtained by averaging the positions of all the cutpoints. Following this, the cutpoints farther than a certain distance from the first estimation are excluded from the next averaging. The process of excluding and averaging was executed several times with gradually shrinking spatial window each time. The diameter of the final spatial window is chosen to minimize the standard deviations of millisecond positions of a stationary tracer. A final window with a radius of 4–8 mm gives the lowest standard deviation, enclosing hundreds to tens of thousands cutpoints in a millisecond, depending on the radioactivity and the location of the particle in the field of view. The cutpoints used for final average, which is taken as the particle position, are referred to as "effective cutpoints".

2.2. The hydrocyclone and experimental rig

The hydrocyclone geometry used in the experiments and CFD simulations is designed to resemble the Stairmand high-efficiency cyclone [18] with a modified inlet and a prolonged cone. Connected with the particle outlet is a particle collection chamber. The dimensions are shown in Figure 5.

The hydrocyclone is incorporated in a flow loop as shown in Figure 6. The entire flow loop is filled with

liquid to avoid development of an air core in the cyclone. A centrifugal pump pushes the liquid, which is water in this study, through the hydrocyclone. After the liquid has been recirculated several times to minimise start-up effects, the radioactive particle is injected, using a syringe, upstream of the pump.

The settling velocity in water shows that the behavior of resin beads of 390–680 μm in the hydrocyclone corresponds to that of 90–115 μm particles with density of 2650 kg/m^3 (the density of sand). The dynamically equivalent diameters of the resin beads are larger than the cut-size of this hydrocyclone, and thus the resin beads are expected to be separated out.

3. CFD SIMULATION

To simulate the highly complex, turbulent, swirling flow field in cyclones, the turbulence model needs to be carefully chosen. The LES (large eddy simulation) turbulence model allows for explicit resolution of the large eddies in a calculation and implicitly accounting for the small eddies by using a subgrid-scale (SGS) model. Derksen et al. [19] used LES turbulence model and achieved a break-through in the simulation of a reverse-flow gas cyclone, reducing the empiricism involved in CFD and allowing modeling of the complex flow phenomena involved. Also, the LES turbulence model has been demonstrated to successfully simulate the transient flow pattern in confined strongly swirling flow in gas swirl tubes [20]. In this study, 3-D LES turbulence model in combination with the SGS model of Smagorinsky was applied using the commercial CFD package Star-CD. Considering the unsteady flow behavior, transient flow calculations have to be implemented. The MARS differencing scheme was applied. The SIMPLE algorithm with temporal discretization of three-time-level implicit was used.

The geometries of hydrocyclone used in experiments and CFD simulations were, as mentioned, identical. The fluid in the hydrocyclone in the simulations was water, of which the properties were: density 997.561 kg/m^3, molecular weight: 18 kg/kmol, and molecular viscosity 8.8871×10^{-4} kg/ms. The number of cells was 331745. Mesh convergence tests were carried out using 775488 cells to assure the validity of solutions. The static pressure distributions simulated under same conditions did not change significantly upon such mesh refinement.

The initial condition in the hydrocyclone was set as no-flow. The no-slip boundary condition was applied at wall boundaries. The initial fluid velocity was set at the cyclone inlet boundary. In the experiments and the simulations, the only fluid outlet was the vortex finder. The mass flow across the outlet conforms to overall continuity.

3-D particle trajectories were calculated using Lagrangian tracking. In Lagrangian particle tracking a particle is followed in the fluid flow field by integrating Newton's second law: $m(d\mathbf{v}/dt) = \sum \mathbf{F}$ with $\mathbf{v}$ the particle velocity, $\sum \mathbf{F}$ the forces acting on the particle due to the fluid or interaction with the wall of the cyclone and m the particle mass. The inlet flow rate, the particle diameter and density were chosen to be close to the experimental conditions.

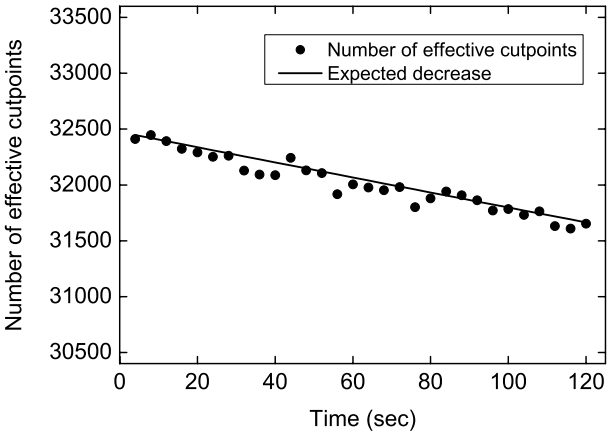

Figure 7. Number of effective cutpoints as the particle stays in water for 120 seconds.

4. RESULTS AND DISCUSSION

4.1. The performance of the labelling method and the particle positioning algorithm

Firstly it was necessary to verify whether the radioactivity would leach off the particle in the water. As the particle moves along with the liquid in the hydrocyclone, measuring the number of effective cutpoints of a moving particle in liquid is preferable. However, considering the number of detected cutpoints is also affected by the position in the field of view, a labelled, stationary resin bead surrounded by water and placed off the center of the field of view was tested. By applying the above-mentioned algorithm (see Sect. 2.1) with a final window of 8 mm to locate the particle, the number of effective cutpoints were found to decrease 3% after 120 s of residence in the water as plotted with dots in Figure 7. Considering the half-life and that the square of the number of cutpoints is proportional to the activity on the particle, the expected decrease can be calculated, plotted as a line in Figure 7. The comparison of measured and expected decrease in the number of cutpoints shows that the decrease is mainly due to the radioactive decay. 120 s is relatively long, since it takes less than 5 s for a tracer particle to traverse the cyclone (see below). Thus the activity on the particle is sufficiently stable during the process investigated in this study.

Although the effective cutpoints slightly decrease, the standard deviations of 4000 positions located once per millisecond do not increase in time during 120 s as shown in Figure 8. The positioning algorithm performs to the same precision during the entire period in spite of the slight decrease in effective cutpoints. Figures 7 and 8 show that when the particle is off the center of field of view (FOV) and with around 32000 effective cutpoints per ms, the standard deviation of less than 330 μm in three directions is achievable. With careful control on the labelling process, the number of effective cutpoint per ms can become as high as around 1.4×10^6, which gives a standard deviation in the particle position below 170 μm in three directions [21].

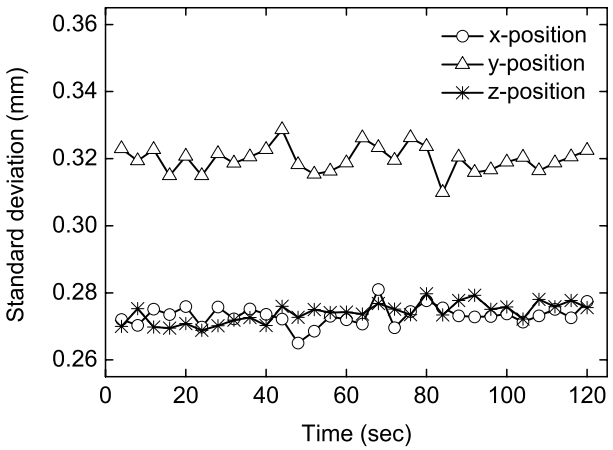

Figure 8. Standard deviation of the position of the particle centroid as a function of time as the particle stays in water for 120 seconds.

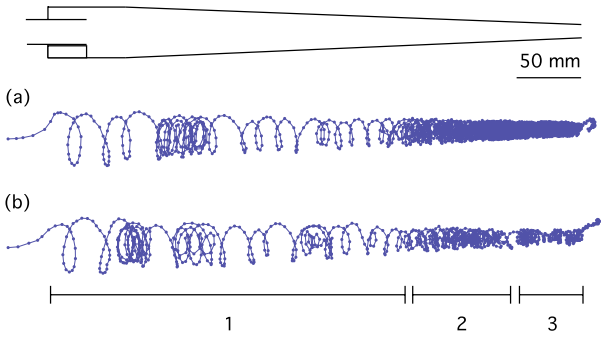

Figure 9. The trajectories of a particle in the hydrocyclone under the same operational condition obtained by PEPT. The numbers of effective cutpoints in each millisecond are in the order of 10^5 and 10^3 in (a) and (b), respectively. In (b) Savitzky-Golay filtering method has been applied on a series of 5 positions with a polynomial order of 2.

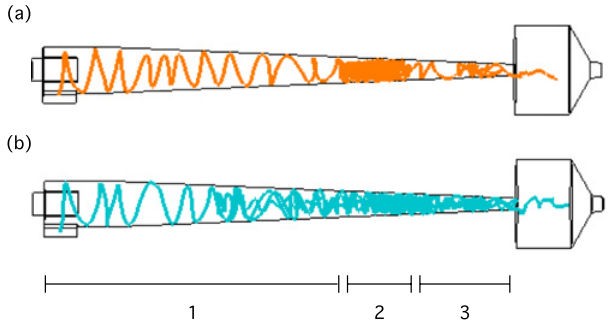

Figure 10. CFD simulated particle trajectory.

4.2. Particle trajectories in the hydrocyclone obtained by PEPT

The trajectory can be drawn after the positions were located once per millisecond, as dotted in Figure 9, using the above-mentioned algorithm. CFD simulated trajectories in Figure 10 have been placed under the experimentally obtained trajectories for convenient comparison (see below).

Figure 9(a) and (b) show the particle trajectories obtained under the same operational condition, where

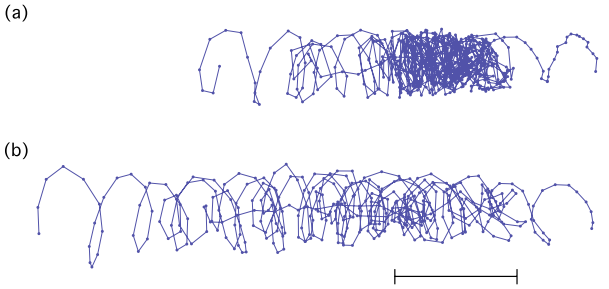

Figure 11. The particle's swirling motion is affected by a strongly turbulent flow down in the hydrocyclone. The bar underneath indicates the turbulent region.

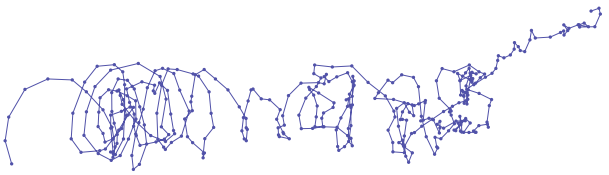

Figure 12. The particle in Figure11(b) has passed the turbulent region and continues spiraling staggeringly.

the numbers of effective cutpoints in each millisecond in Figure 9(a) and (b) are in the order of 10^5 and 10^3, respectively. Figure 9(b) was obtained after applying Savitzky-Golay filtering method [22] using a series of 5 positions with a polynomial order of 2, which shows the capability of tracking a low-radioactive and off-centered (relatively in the FOV) particle by combining the positioning algorithm and Savitzky-Golay filtering method to filter out the positioning inaccuracy.

The track in Figure 9(a) seems denser than that in Figure 9(b). However, investigating the characteristics of the tracks shows identical behaviors. The particle flow in the hydrocyclone can be divided into three stages: In the first stage as approximately indicated below Figure 9, the particle's regular swirling motion toward the underflow outlet is clearly visible, except that in some short time intervals the particle appears to move into the inner, upward flowing vortex and reverses its axial direction, whereafter it is soon centrifuged outward to the downwardly directed vortex again.

In the second stage, when the particle reaches the lower part of the conical section the trajectory traces seem much denser. The particle spends a long time around a specific region. Following the particle in this section shows that the particle was affected by a strongly turbulent flow at a specific axial position as indicated below Figure 11, experiencing disorganized motion and being pulled into the inner vortex for several times. Figure 11(a) and (b) present this turbulent region of Figure 9(a) and (b), respectively. After escaping from the turbulent region, the particle regains its swirling motion, but moves and rotates much slower, indicated by the successive positions being much closer on the trajectory.

In the third stage, the particle, having passing the turbulent region the first time, continues its slower spiraling path and often loses its direction and spiral pattern as shown in Figure 12, which is the third stage of Figure 9(b). The third stage of the trajectory in Figure 9(a)

is not shown since the track is too dense so that no details can be seen. In the third stage of Figure 9(a) the particle swirls slowly, being frequently pulled into the inner vortex and in many times swirling upward to upstream of the turbulent section. Many times of the flow reversals and particle's experiencing the turbulent section make the track very dense. The axial flow reversals occur repeatedly, resulting in a long residence time in this region. As the particle spends such a long time swirling back and forth below and around the turbulent region, the separation and the transport of the particles along the wall will be ineffective in this region.

Similar phenomena were observed in all six experiments under the same conditions as those of Figure 9. The differences are in the number of times for which the particle was pulled into the inner vortex in stage 2 and stage 3, and the distance for which the particle flows upwardly. The residence time in six experiments therefore varied in the range of 0.8–4.8 s.

4.3. CFD simulations: Static pressure distribution and Lagrangian particle tracking

The 3-D particle trajectory shown in Figure 10 was generated using Lagrangian tracking in the fluid field calculated using the LES turbulence model. The particle shown here was injected at 6.7 sec after the beginning of the simulation. The simulated trajectories show very dense tracks in stage 2 as indicated in Figure 10. Magnification of these dense sections reveals similar phenomena to those found in experiments, e.g. disorganized tracks, the particle being pulled into the inner vortex, and slow and erratic transportation below this turbulent region.

The simulated static pressure distributions are presented below to help understand the root cause for this phenomenon.

Cross-sectional contour plots of static pressure at different simulation time for inlet velocity of 4 m/s are shown in Figure 13. As can be seen, the vortex core bends to the wall and rotates on the wall as it forms. Gradually, the vortex core swirls downward, but stops descending and rotates at some level above the underflow outlet. The cross-sectional static pressure distribution and the axial position of the core attachment did not change significantly after 5.5 sec of simulation. This phenomenon is known as the "end of the vortex" [11]. As the phenomenon occurs, three rotations appear in cyclone: one around the core of the vortex and another is the vortex core's rotating on the wall, which then induces a much weaker secondary vortex below the "end of the vortex".

The comparison and superposition of particle trajectory on the static pressure shows a strong correlation between the particle behaviors and the "end of the vortex". The trajectory in Figure 10(a) is further analyzed in Figure 14, where the particle was injected at a small radius. Figures 14(a) and (b) show that a dense track appears around the vortex core's axial position of attachment to the wall, which is indicated by an arrow in the graph. Figures 14(c) and (d) shows that the particle swirls close to the core-attached position, and then is dragged into the inner vortex, flowing upwardly. Such process occurs

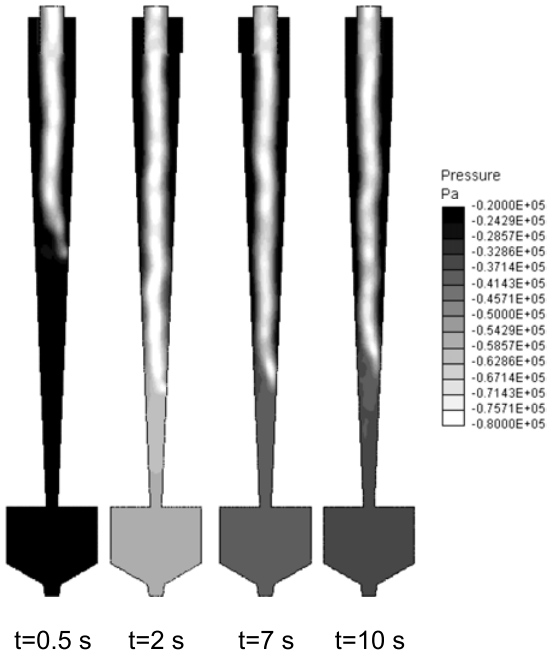

Figure 13. The cross-sectional contour plots of static pressure simulated at inlet velocity of 4 m/s.

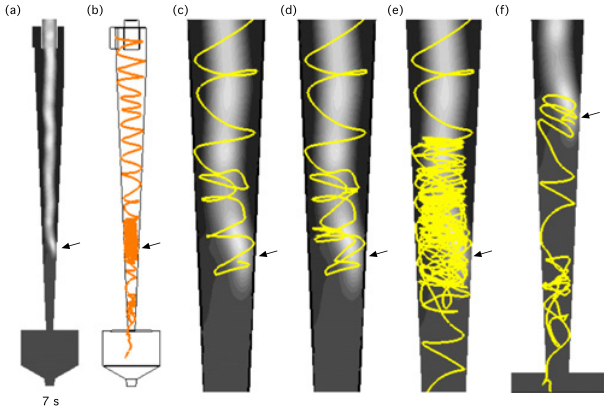

Figure 14. The correlation between the particle behavior and the "end of the vortex". The position on the wall where the vortex core bends and attaches is indicated by an arrow. (a) The contour plot of static pressure showing the core attached to the wall at the axial position of the "end of the vortex". (b) The whole particle track. (c)-(e) Detail showing the particle passing the "end of the vortex": The particle drawn into the upward inner vortex and centrifuged out again for several times. (f) The particle experiencing weak swirling and further axial flow reversals after escaping from the "end of the vortex".

several times, which causes the very dense track as shown in Figure 14(e). In Figure 14(f) the particle has left the "end of the vortex" region, transported in the induced, much weaker, secondary vortex, and occasionally runs arbitrarily, which resembles those found in the PEPT trajectory as shown in Figure 12.

Figure 15 presents the comparison and superposition of particle trajectory in Figure 10(b) on the static pressure. The particle was injected in the center of the inlet. In Figure 15(c) the particle suddenly loses its original swirling pace near and below the core-attached position, and in Figure 15(d) the particle trajectory from entering

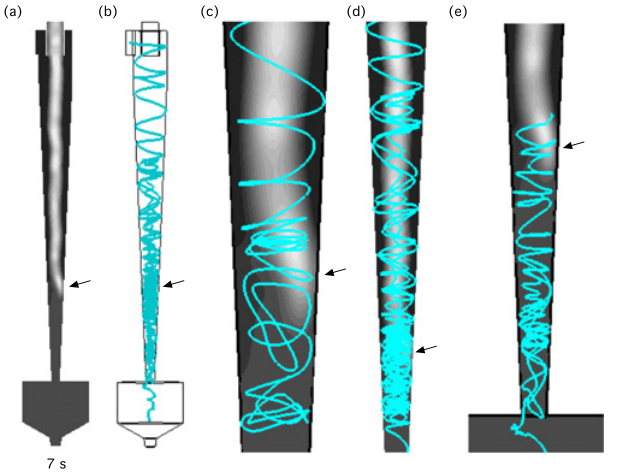

Figure 15. The correlation between the particle behavior and the "end of the vortex". The position on the wall where the vortex core bends and attaches is indicated by an arrow. (a) The contour plot of static pressure showing the core attached to the wall at the axial position of the "end of the vortex". (b) The whole particle track. (c)-(d) Detail showing the particle passing the "end of the vortex": The particle trapped by the "end of the vortex", moving at a disordered pace, drawn into the upward inner vortex, and centrifuged out again. (e) The particle experiencing weak swirling and further axial flow reversals after escaping from the "end of the vortex".

to leaving the "end of the vortex" region shows that the particle flow upwardly for a longer distance compared to Figure 14(e). After leaving the "end of the vortex" region, the particle flows upwardly a few times before finally entering the particle collection chamber, which corresponds to the particle behavior found in the third stage of the PEPT trajectory in Figure 9(a).

In the simulations of 120 particles, all the trajectories are obviously affected by the "end of the vortex" whether the particle is injected well within the inlet or close to the cyclone wall. The differences, resembling those in PEPT experiments, are in the number of times the particle is pulled into the inner vortex, and the distance that the particle flows upwardly each time. The residence time of the simulated particle in the hydrocyclone shown in Figure 14 and Figure 15 is approximately 1 sec. In the cases where more flow reversals take place, the residence times increase correspondingly.

These magnified sections together with the static pressure distribution show that the particle behaviors obtained by PEPT and CFD simulations are very similar, although the simulated "end of the vortex" position is higher than that observed in the experiments possibly because the wall friction has not been simulated precisely. As demonstrated by the CFD simulations, the "end of the vortex" phenomenon was found to be the likely cause for the irregular path of the particle in the lower section of the hydrocyclone.

5. CONCLUSION

In this study, particle tracking by the "PEPT" technique with high temporal and spatial resolutions has been accomplished and utilized to study the flows of particles in a hydrocyclone. Several interesting and unexpected events have been observed in the trajectory. The numerically calculated particle trajectories obtained by Lagrangian tracking in a LES simulated fluid field correspond to the experimental results very well. Further investigation into the simulated static pressure distributions reveals that the "end of the vortex" phenomenon caused the particle to flow irregularly and caused difficulties for the particle separation in the lower section of the hydrocyclone.

High precision PEPT has been demonstrated to be an invaluable tool for 3-D particle tracking and CFD simulation verification. Since solids, oil droplets, and gas bubbles may all be labelled, PEPT can be further developed for studying flows of various media in diverse processes.

The authors would like to thank the mechanical workshop at the University of Bergen and the Centre for Nuclear Medicine at Haukeland University Hospital for help with the experimental setup and procedure. Also Siemens Molecular Imaging is appreciated for help with interpreting the list-mode data. The Petromaks program by the Norwegian Research Council and Aker Solutions are acknowledged for funding this work. The Akademia program by Statoil is appreciated for funding the conference presentation.

References

[1] F. Depypere, J.G. Pieters, K. Dewettinck, Journal of Food Engineering **93**(3), 324 (2009)
[2] S. Fitzpatrick, Y. Ding, C. Seiler, C. Lovegrove, S. Booth, R. Forster, D. Parker, J. Seville, Pharmaceutical Technology pp. 70–78 (2003)
[3] W.D. Griffiths, D.J. Parker, X. Fan, M. Hausard, Materials Science and Technology **26**(5), 528 (2010)
[4] P.G. Fairhurst, M. Barigou, P.J. Fryer, J.P. Pain, D.J. Parker, International Journal of Multiphase Flow **27**(11), 1881 (2001)
[5] A. Ingram, M. Hausard, X. Fan, D.J. Parker, J.P.K. Seville, N. Finn, R. Kilvington, M. Evans, *Portable Positron Emission Particle Tracking (PEPT) for Industrial Use*, in *Proceedings of 12th International Conference on Fluidization* (2007), pp. 13–17
[6] R.D. Wildman, J.M. Huntley, D.J. Parker, Physical Review Letters **86**(15), 3304 (2001)
[7] A.C. Hoffmann, L.E. Stein, *Gas cyclones and swirl tubes: principles, design and operation* (Springer, 2007), ISBN 3-540-43326-0
[8] L. Svarovsky, M.T. Thew, eds., *Hydrocyclones: analysis and applications* (Kluwer Academic Publishers, Boston, 1992), ISBN 0-7923-1876-5
[9] S.R. Knowles, D.R. Woods, I.A. Feuerstein, The Canadian Journal of Chemical Engineering **51**(3), 263 (1973)
[10] Z.B. Wang, L.Y. Chu, W.M. Chen, S.G. Wang, Chemical Engineering Journal **138**(1-3), 1 (2008)
[11] W. Peng, A.C. Hoffmann, H.W.A. Dries, M.A. Regelink, L.E. Stein, Chemical Engineering Science **60**(24), 6919 (2005)

[12] K.T. Hsieh, R.K. Rajamani, AIChE Journal **37**(5), 735 (1991)
[13] T. Neesse, F. Donhauser, *Advances in the theory and practice of hydrocyclone technique*, in *Proceedings of the XXI International Mineral Processing Congress*, edited by P. Massacci (Elsevier, 2000), pp. A4-69–A4-76
[14] J. Cullivan, R. Williams, R. Cross, Chemical Engineering Research and Design **81**(4), 455 (2003)
[15] I.H. Yang, C.B. Shin, T.H. Kim, S. Kim, Minerals Engineering **17**(5), 637 (2004)
[16] D.L. Bailey, D.W. Townsend, P.E. Valk, M.N. Maisey, eds., *Positron emission tomography: basic sciences* (Springer, 2005), ISBN 1-85233-798-2
[17] A.C. Hoffmann, C. Dechsiri, F. van de Wiel, H. Dehling, Measurement Science and Technology **16**(3), 851 (2005)
[18] C. Stairmand, Transactions of the Institution of Chemical Engineers **29**, 356 (1951)
[19] J.J. Derksen, H.E.A. Van den Akker, AIChE Journal **46**(7), 1317 (2000)
[20] G.I. Pisarev, A.C. Hoffmann, W. Peng, H.A. Dijkstra, Applied Mathematics and Computation **217**(11), 5016 (2011)
[21] Y.-F. Chang, C.G. Ilea, Ø.L. Aasen, A.C. Hoffmann, Chemical engineering Science **66**(18), 4203 (2011)
[22] A. Savitzky, M.J.E. Golay, Analytical Chemistry **36**(8),1627 (1964)